Research Article

Application of hybrid control algorithm on the vehicle active suspension system to reduce vibrations

Tuan Anh Nguyen[1] ⓘ, Jamshed Iqbal[2],
Thi Thu Huong Tran[3] and Thang Binh Hoang[3]

Abstract

This research proposes a hybrid control algorithm to enhance smoothness in a vehicle's motion. The control signal is synthesized from two separate controllers, Proportional Integral Derivative (PID) and Sliding Mode Control (SMC), to achieve superior control performance. The novelty of the proposed control algorithm lies in using a double-loop algorithm to determine the controller parameters. The algorithm proposed in this research involves two computational processes to determine the model's optimal values including the raw value and the acceptable value. The proposed control algorithm has been simulated considering three specific cases corresponding to the three types of road stimuli. The results demonstrate that the values of sprung mass displacement and acceleration dropped considerably with the application of the proposed algorithm. Moreover, the change in vertical force at the wheel is also reduced with the application of the algorithm particularly in the third case where the vertical force at the wheel has reached to zero. The average values of vehicle body displacement are found to be 166.17 mm (for passive case), 54.20 mm (for PID), and 42.52 mm (for SMC). The proposed control algorithm managed to reduce this value to 8.95 mm as evidenced by simulation results. Finally, the response of the control system when subjected to an excitation signal from the road surface further demonstrates efficacy of the proposed hybrid control algorithm.

Introduction

The roughness of a road can cause oscillations in a moving vehicle causing uncomfortability to the onboard passengers.[1] Moreover, in case of shipping and logistics vehicles, the quality of the goods may be affected. There are several parameters used to evaluate oscillations in vehicles including but not limited to[2]; change in the vehicle's body displacement, acceleration, and the difference in a wheel vertical force. For single impulse or discontinuous oscillations, the maximum values of the aforementioned parameters need to be

[1]Faculty of Mechanical Engineering, Thuyloi University, Hanoi, Vietnam
[2]School of Computer Science, Faculty of Science and Engineering, University of Hull, Hull, UK
[3]School of Mechanical Engineering, Hanoi University of Science and Technology, Hanoi, Vietnam

Corresponding author:
Tuan Anh Nguyen, Faculty of Mechanical Engineering, Thuyloi University, 175 Tay Son, Dong Da, Hanoi 100000, Vietnam.
Email: anhngtu@tlu.edu.vn

taken into account. On the other hand, the continuous or periodic oscillations involve consideration of their average values.

The oscillations in a vehicle can be kept under control with the help of a suspension system. Each kind of a suspension system requires a different set of parts. A passive suspension system utilizes metal springs and standard dampers. The stiffness of these components remains unchanged. Therefore, smoothness in a vehicle's motion cannot be guaranteed. In order to resolve the vehicle's oscillation issues, it is necessary to vary the stiffness of spring and damper. Nguyen[3] introduced an air suspension system, which uses variable stiffness air springs. Variations in internal pneumatic pressure affect the spring's stiffness.[4,5] Besides, the suspension system using a magnetorheological damper helps to improve the vehicle's stability during its motion. The magnetorheological damper uses electromagnetic force to regulate the flow of internally circulated liquid, thus making it possible to flexibly change the oscillation quenching process.[6,7] Active suspension systems should be used to mitigate oscillations more flexibly.[8–10] An active suspension system contains an extra hydraulic actuator that works based on the opening and closing of the servo valves. These valves operate when a control signal is received from the controller.[11] In general, an active suspension system demonstrates superior performance as compared to other suspension systems. The performance of an active suspension system depends on the underlying control algorithm. The controllers can be divided into several types: linear control, nonlinear control, intelligent control, adaptive control, etc.

For simple control problems, the plant is often assumed to be linear and thus a Proportional Integral derivative (PID) algorithm can be used in case of a Single Input Single Output (SISO) system. The PID controller consists of three operations, each having a corresponding coefficient.[12] The tuning of these coefficients is critical. Mohammadikia and Aliasghary[13] proposed a method to adjust the PID controller's coefficients based on fuzzy rules. The proposed fuzzy algorithm consisted of one input and two outputs. The defuzzification process was designed based on experience and experiments. In general, the membership functions in fuzzy algorithms are triangular, trapezoidal, or Gaussian.[14] Fuzzy algorithms can be divided into smaller layers corresponding to the three operations of the PID controller.[15] Additionally, particle swarm methods may be employed to tune and configure the PID controller.[16–19] If two quantities of a plant (such as displacement and acceleration) need to be controlled, two PID controllers can be combined.[20] However, this may cause unwanted couplings and interactions. Park and Yim[21] used the Linear Quadratic Regulator (LQR) algorithm to dynamically control an active suspension system using a quarter-model by optimizing the cost function.[22] The state space model of the vehicle under oscillations was written in the form of a matrix representing system states to solve the Riccati algebraic equation.[23] When a LQR controller is further integrated with the cancellation term, it becomes intelligent (i-LQR) as introduced by Haddar.[24] However, the effectiveness of the above algorithms is not guaranteed when applying them to control the systems having nonlinear oscillation. Therefore, these algorithms should be replaced or combined with more complex nonlinear control techniques.

Sliding Mode Control (SMC) algorithm is often used for plants that have nonlinear or random stimuli.[25] The control algorithm relies on Lyapunov theory to design the asymptotically stable controllers.[26] The quantity being controlled is driven onto the sliding manifold to achieve a steady state.[27] The sliding manifold in the present work, has been developed using the higher order derivatives based on the derived model reported in Nguyen et al.[28] Therefore, it is necessary to linearize the actuator dynamics into an approximate linear differential equation as highlighted in Nguyen.[29] The order of the derivative signal depends on the system order. The model becomes more complex and sophisticated for systems with several state variables.[30] SMC algorithm inherently suffers from chattering phenomenon leading to noisy control signals.[31–33] The fuzzy algorithm can be combined with SMC algorithm to form a "hybrid controller" to solve this problem.[34] Other advanced control algorithms used in control of an active suspension are reported in References 35–39. In general, the effectiveness of these methods is outstanding.

Based on the abovementioned discussion, the SMC algorithm can help reduce suspension system oscillations. However, it inherently suffers from the "chattering" phenomenon, negatively affecting the system's performance resulting in an oscillatory behavior. A SMC algorithm can be highly effective when applied to control a specific object. If the system has several parameters that need to be controlled, we may need to use multiple SMC algorithms. However, combining the algorithms may be computationally more complex and expensive. On the other hand, we cannot achieve ideal performance level with a single sliding mode controller.

The PID controller is quite simple, computationally inexpensive, and highly systematic. With real-time control capabilities, the PID controller has been the main workhorse in industry for decades and is suitable for dynamic systems with varying conditions. However, they are sensitive to noise and measurement errors.

Given the pros and cons of each of PID and SMC based laws, formulating an integrated controller by combining PID and SMC will provide opportunity to get benefits from both control techniques. This results in obtaining superior control performance compared to

individually applying each of the aforementioned control technique. In addition, the "chattering" phenomenon can be largely eliminated and the algorithm design process becomes simpler compared to using two integrated SM controllers. Finally, the proposed hybrid control approach can be widely applied in various applications, thanks to the systematic characteristics of the PID algorithm.

This research proposes a PID-SMC hybrid control method to improve the performance of the active suspension system. The final control signal is synthesized by integrating the two-component signals during the design process. The novelty of the proposed control law relies on harnessing prominent features of both controllers; PID and SMC. Moreover, in contrast to most of the reported studies for example, References 23, 40–42, which used a single loop algorithm to determine the optimal values of the controller parameters, the present study introduces a novel double-loop method to estimate the required parameters more accurately.

The remaining article is organized in four sections; Section "Dynamic model and controller design" presents dynamics of a quarter-model and the proposed control algorithm. Simulation results are discussed in Section "Simulation results." Finally, Section "Conclusion" comments on conclusion and briefly mention the future work.

Dynamic model and controller design

There are several types of dynamic models commonly used to simulate vehicle oscillations. For vehicle control problems, dynamics of a quarter-model is often used, which includes the hydraulic actuator as illustrated in Figure 1. The separation between sprung and unsprung masses is also shown. Motion of the two masses can be formulated as in (1, 2) based on the D'Alembert principle.

$$m_s \frac{dz_s^2}{dt^2} = F_S + F_D + F_A \tag{1}$$

$$m_u \frac{dz_u^2}{dt^2} = F_T - F_S - F_D - F_A \tag{2}$$

where m_s is sprung mass, m_u is unsprung mass, F_s is spring force, F_D is damper force, F_A is actuator force, F_T is tire spring force, z_s is sprung mass displacement, and z_u is unsprung mass displacement.

The spring force, damping force, and tire force can be respectively given by (3)–(5).

$$F_S = S(z_u - z_s) \tag{3}$$

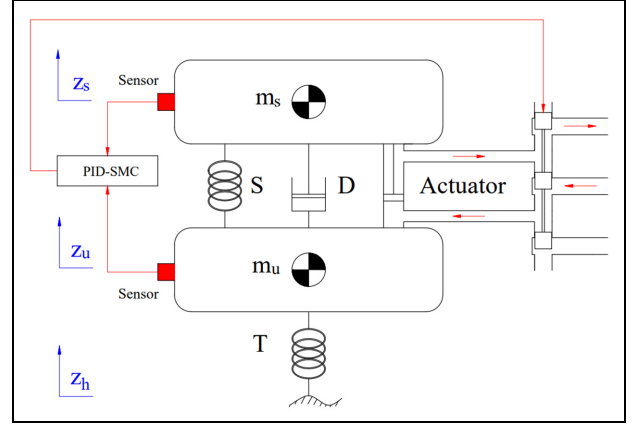$$F_D = D\left(\frac{dz_u}{dt} - \frac{dz_s}{dt}\right) \tag{4}$$

Figure 1. Dynamics of the quarter-model.

$$F_T = T(z_h - z_u) \tag{5}$$

where S is spring coefficient, D is damper coefficient, and T is tire spring coefficient.

The force generated by the actuator is determined by the linearized equation given in (6)

$$\frac{dF_A}{dt} = \gamma_1 u(t) - \gamma_2 F_A - \gamma_3\left(\frac{dz_u}{dt} - \frac{dz_s}{dt}\right) \tag{6}$$

where γ_1, γ_2, and γ_3 are coefficients.

Given the nonlinear nature of the vehicular system, a robust and nonlinear control algorithm, SMC is proposed and is applied to this model.

Let $e_1(t)$ be the error between the setpoint signal $y_{s1}(t)$ and the output signal $y(t)$. That is,

$$e_1(t) = y_{s1}(t) - y_1(t) \tag{7}$$

For the system to be stable, the error signal $e_1(t)$ must approach to zero. This value will oscillate around the sliding surface and move toward a stable position as illustrated in Figure 2.

To simplify the problem, a linear sliding surface (8) is often used.[43]

$$s(e) = \vartheta_0 e + \vartheta_1 \frac{de}{dt} + \vartheta_2 \frac{d^2 e}{dt^2} \dots + \vartheta_{n-2}\frac{d^{n-2}e}{dt^{n-2}} + \frac{d^{n-1}e}{dt^{n-1}} \tag{8}$$

The coefficients ϑ_i in (8) must be the coefficients of the polynomial $P(p)$ given in (9) such that $P(p)$ is a Hurwitz polynomial.

$$P(p) = \vartheta_0 + \vartheta_1 p + \vartheta_2 p^2 + \dots + \vartheta_{n-2}p^{n-2} + p^{n-1} \tag{9}$$

The sliding condition of the control problem to bring the error to zero systematically is given in (10).

$$\frac{ds}{dt}sgn(s) < 0 \tag{10}$$

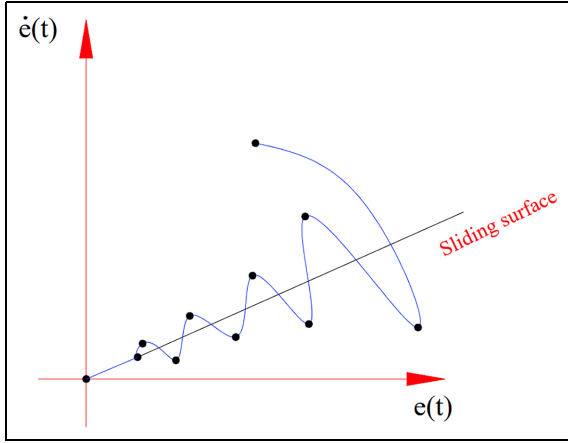**Figure 2.** Sliding surface.

Consider a nonlinear plant of order n with the model given in (11) as,

$$\begin{cases} \dfrac{dx_1}{dt} = x_2 \\[6pt] \dfrac{dx_2}{dt} = x_3 \\[6pt] \dots \\[6pt] \dfrac{dx_{n-1}}{dt} = x_n \\[6pt] \dfrac{dx_n}{dt} = f(x_1, x_2, ..., x_n) + u_1(t) \end{cases} \qquad (11)$$

Assuming that the output of the model is a state variable,

$$y_1(t) = x_1 \qquad (12)$$

From (8), the sliding surface $s(e)$ can be rewritten as in (13),

$$s(e) = \sum_{i=0}^{n-1} \vartheta_i \frac{d^i e}{dt^i} = \sum_{i=0}^{n-1} \vartheta_i \frac{d^i y_{sp1}}{dt^i} - \sum_{i=0}^{n-1} \vartheta_i \frac{d^i y_1}{dt^i} \qquad (13)$$

Let

$$\overline{y_{s1}} = \sum_{i=0}^{n-1} \vartheta_i \frac{d^i y_{s1}}{dt^i} \qquad (14)$$

The sliding function (13) becomes,

$$s(e) = \overline{y_{s1}} - \sum_{i=0}^{n-1} \vartheta_i x_{i+1} \qquad (15)$$

Substituting (15) in (10), we obtain,

$$\left(\frac{d\overline{y_{s1}}}{dt} - \sum_{i=0}^{n-1} \vartheta_i \frac{dx_{i+1}}{dt} \right) sgn(s) < 0 \qquad (16)$$

If the setpoint signal y_{s1} is constant, that is,

$$\frac{d\overline{y_{s1}}}{dt} = 0 \qquad (17)$$

The control signal $u_1(t)$ gets the form given in (18),

$$u_1(t) = - \left(\sum_{i=0}^{n-2} \vartheta_i x_{i+2} + f(x_1, x_2, ..., x_n) \right) + sgn(s) \qquad (18)$$

SMC technique is applied to the suspension system model with five state variables x_1 to x_5 given in (19) as,

$$\begin{aligned} x_1 &= z_s \\ x_2 &= \frac{dz_s}{dt} \\ x_3 &= z_u \\ x_4 &= \frac{dz_u}{dt} \\ x_5 &= F_A \end{aligned} \qquad (19)$$

Taking the derivative of the variables given in (19), we obtain (20) as,

$$\begin{aligned} \frac{dx_1}{dt} &= x_2 \\ \frac{dx_2}{dt} &= \frac{1}{m_s}(-Sx_1 - Dx_2 + Sx_3 + Dx_4 + x_5) \\ \frac{dx_3}{dt} &= x_4 \\ \frac{dx_4}{dt} &= \frac{1}{m_u}(Sx_1 + Dx_2 - (S+T)x_3 - Dx_4 - x_5) \\ \frac{dx_5}{dt} &= -\gamma_3 x_2 + \gamma_3 x_4 - \gamma_2 x_5 + \gamma_1 u(t) \end{aligned} \qquad (20)$$

Taking the first to the fifth derivative of the output signal.

$$\frac{dy_1}{dt} = \frac{dx_1}{dt} = x_2 \qquad (21)$$

$$\frac{d^2 y_1}{dt^2} = -\frac{T}{\chi m_1} x_3 \qquad (22)$$

$$\frac{d^3 y_1}{dt^3} = -\frac{T}{\chi m_1} x_4 \qquad (23)$$

$$\frac{d^4 y_1}{dt^4} = -\frac{T}{\chi m_s m_u}(Sx_1 + Dx_2 - (S+T)x_3 - Sx_4 - x_5) \qquad (24)$$

$$\frac{d^5y_1}{dt^5} = \frac{T}{\chi m_s m_u} \begin{pmatrix} SD(m_s^{-1} + m_u^{-1})x_1 \\ + (D^2 m_s^{-1} + D^2 m_u^{-1} - S - \gamma_3)x_2 \\ + D(-Sm_s^{-1} - (S+T)m_u^{-1})x_3 \\ + (-D^2 m_s^{-1} - D^2 m_u^{-1} + (S+T) + \gamma_3)x_4 \\ + (-Dm_s^{-1} - Dm_u^{-1} - \gamma_2)x_5 \end{pmatrix}$$
$$+ \frac{T\gamma_1}{\chi m_s m_u}u_1(t) \tag{25}$$

(25) can be rewritten as follows,

$$\frac{d^5y_1}{dt^5} = a_1 \sum_{n=1}^{5} b_n x_n + a_2 u_1(t) \tag{26}$$

where,

$$a_1 = T\chi^{-1}m_s^{-1}m_u^{-1}$$
$$a_2 = T\gamma_1\chi^{-1}m_s^{-1}m_u^{-1}$$
$$b_1 = SD(m_s^{-1} + m_u^{-1})$$
$$b_2 = D^2(m_s^{-1} + m_u^{-1}) - S - \gamma_3$$
$$b_3 = -D(Sm_s^{-1} + (S+T)m_u^{-1})$$
$$b_4 = -D^2(m_s^{-1} + m_u^{-1}) + (S+T) + \gamma_3$$
$$b_5 = -D(m_s^{-1} + m_u^{-1}) - \gamma_2$$

The sliding surface (15) becomes (27),

$$s(e_1) = \sum_{n=0}^{4} \vartheta_n \frac{d^{4-n}e_1}{dt^{4-n}} = \frac{d^4e_1}{dt^4} + \vartheta_1 \frac{d^3e_1}{dt^3} + \vartheta_2 \frac{d^2e_1}{dt^2}$$
$$+ \vartheta_3 \frac{de_1}{dt} + \vartheta_4 e_1 \tag{27}$$

The control law $u_1(t)$ is chosen according to (28).

$$u_1(t) = \frac{1}{a_2}\left(-a_1 \sum_{n=1}^{5} b_n x_n + \frac{d^5y_{s1}}{dt^5} + \vartheta_1 \frac{d^4e_1}{dt^4} + \vartheta_2 \frac{d^3e_1}{dt^3}\right.$$
$$\left. + \vartheta_3 \frac{d^2e_1}{dt^2} + \vartheta_4 \frac{de_1}{dt} + Psgn\left(\sum_{n=0}^{4} \vartheta_n \frac{d^{4-n}e_1}{dt^{4-n}}\right)\right) \tag{28}$$

where P is a positive coefficient.

Stability proof

The Lyapunov control function given in (29) is a positive definite function $\forall x \neq 0$.

$$V(x) = \frac{1}{2}s^2 > 0 \forall x \neq 0 \tag{29}$$

Taking the derivative of (29), we obtain (30),

$$\frac{dV(x)}{dt} = s\frac{ds}{dt} \tag{30}$$

Taking the fifth derivative of (7), we get (31). Then, taking the derivative of (27), we get (32),

$$\frac{d^5e_1}{dt^5} = \frac{d^5y_{s1}}{dt^5} - \frac{d^5y_1}{dt^5} \tag{31}$$

$$\frac{ds}{dt} = \frac{d^5e_1}{dt^5} + \vartheta_1 \frac{d^4e_1}{dt^4} + \vartheta_2 \frac{d^3e_1}{dt^3} + \vartheta_3 \frac{d^2e_1}{dt^2} + \vartheta_4 \frac{de_1}{dt} \tag{32}$$

Combining equations (31) and (32), we get (33),

$$\frac{ds}{dt} = \frac{d^5y_{s1}}{dt^5} - \frac{d^5y_1}{dt^5} + \vartheta_1 \frac{d^4e_1}{dt^4} + \vartheta_2 \frac{d^3e_1}{dt^3} + \vartheta_3 \frac{d^2e_1}{dt^2} + \vartheta_4 \frac{de_1}{dt} \tag{33}$$

Substituting (26) into (33) results in (34),

$$\frac{ds}{dt} = \frac{d^5y_{s1}}{dt^5} - a_1 \sum_{n=1}^{5} b_n x_n - a_2 u_1(t) + \vartheta_1 \frac{d^4e_1}{dt^4}$$
$$+ \vartheta_2 \frac{d^3e_1}{dt^3} + \vartheta_3 \frac{d^2e_1}{dt^2} + \vartheta_4 \frac{de_1}{dt} \tag{34}$$

Combining (28) and (34), we obtain (35),

$$\frac{ds}{dt} = \frac{d^5y_{s1}}{dt^5} - a_1 \sum_{n=1}^{5} b_n x_n - a_2 u_1(t) + \vartheta_1 \frac{d^4e_1}{dt^4}$$
$$+ \vartheta_2 \frac{d^3e_1}{dt^3} + \vartheta_3 \frac{d^2e_1}{dt^2} + \vartheta_4 \frac{de_1}{dt}$$
$$= \frac{d^5y_{s1}}{dt^5} - a_1 \sum_{n=1}^{5} b_n x_n$$
$$- a_2\left[\frac{1}{a_2}\left(-a_1 \sum_{n=1}^{5} b_n x_n + \frac{d^5y_{s1}}{dt^5} + \vartheta_1 \frac{d^4e_1}{dt^4} + \vartheta_2 \frac{d^3e_1}{dt^3}\right.\right.$$
$$\left.\left. + \vartheta_3 \frac{d^2e_1}{dt^2} + \vartheta_4 \frac{de_1}{dt} + Psgn\left(\sum_{n=0}^{4} \vartheta_n \frac{d^{4-n}e_1}{dt^{4-n}}\right)\right)\right]$$
$$+ \vartheta_1 \frac{d^4e_1}{dt^4} + \vartheta_2 \frac{d^3e_1}{dt^3} + \vartheta_3 \frac{d^2e_1}{dt^2} + \vartheta_4 \frac{de_1}{dt}$$
$$= -Psgn\left(\sum_{n=0}^{4} \vartheta_n \frac{d^{4-n}e_1}{dt^{4-n}}\right)$$
$$= -Psgn(s) \tag{35}$$

Substituting (35) into (30) finally results in (36),

$$\frac{dV(x)}{dt} = -Psgn(s)s < 0 \quad \forall x \neq 0 \tag{36}$$

According to (29) and (36), the system reaches a steady state.
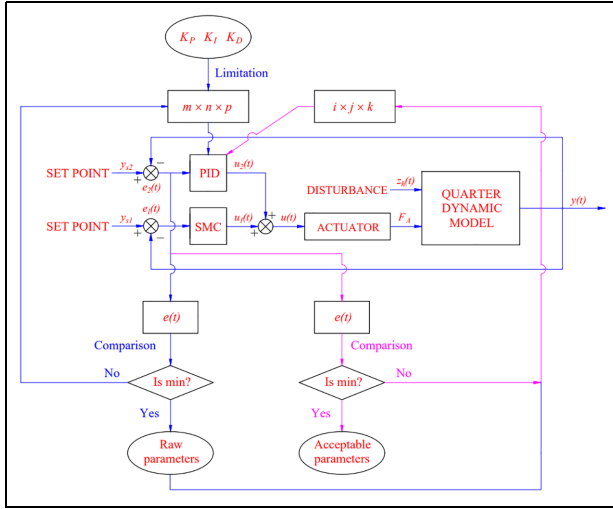
Figure 3. Schematic of the proposed hybrid PID-SMC algorithm.

The proposed hybrid PID-SMC controller is shown in Figure 3, which optimizes the system's overall performance. The double-loop method must undergo two steps to determine the raw and acceptable values. The raw value is determined from the first loop with wider steps. However, the accuracy is not high. Therefore, it is necessary to introduce the second loop with finer steps to compute accurate values (Figure 3). The system's stability is evidenced by choosing optimal values of the PID controller. These values are selected so as to minimize the system error. This process is performed in two loops.

Let $e_2(t)$ be the error signal corresponding to the PID controller.

$$e_2(t) = y_{s2}(t) - y_2(t) \tag{37}$$

The control signal $u_2(t)$ is determined using (38) as,

$$u_2(t) = K_P e_2(t) + K_I \int_0^t e_2(\tau)d\tau + K_D \frac{de_2(t)}{dt} \tag{38}$$

The overall control signal of the hybrid controller is given by (39) as,

$$u(t) = u_1(t) + u_2(t) \tag{39}$$

Several methods can be used to determine the parameters of the PID controller, such as using the Ziegler Nichols method, Genetic Algorithm (GA) solution, fuzzy set or Particle Swarm Optimization (PSO) algorithm, etc. In this study, we propose a double-loop algorithm for determining the PID controller parameters. As illustrated in Figure 3, the algorithm consists of two processes: (i) Define raw values of the controller

parameters, (ii) Determine their acceptable values. In terms of the first process, the limits of the parameters need to be predefined. The values within the range are used to run simulations for the vibration problem. The corresponding output values are obtained for each parameter, including vehicle body displacement and acceleration and error signal $e(t)$. The algorithm selects the controller's parameters that result in minimal error signal. Based on this criterion, the optimal value can be determined. Assuming that in the limited range of parameters, there are m parameters of K_P, n parameters of K_I, and p parameters of K_D, the number of cases to run the simulation is equal to the product $m \times n \times p$. Therefore, the number of simulation runs will be huge if the division of the range of values is small. We can use a reasonable division to find the required parameters to overcome this problem. However, the raw value needs to be accurate.

The second process involves determining the acceptable values. The fine value is determined from the original raw value obtained from the first process. The division of this range is smaller ($i \times j \times k$) to ensure accuracy.

The double-loop optimization algorithm is mathematically formulated in (40) and (41), which respectively correspond to the first process and the second process.

$$
\begin{aligned}
&for \quad \begin{cases} K_P = m_{min} : m : m_{max} \\ K_I = n_{min} : n : n_{max} \\ K_D = p_{min} : p : p_{max} \end{cases} \\
&if \quad e(t) = e(t)_{min} \\
&\qquad \begin{cases} K_{Po} = K_{Praw} \\ K_{Io} = K_{Iraw} \\ K_{Do} = K_{Draw} \end{cases} \\
&else \quad \begin{cases} K_P = K_{Po+m} \\ K_I = K_{Io+n} \\ K_D = K_{Do+p} \end{cases}
\end{aligned} \tag{40}
$$

$$
\begin{aligned}
&for \quad \begin{cases} K_P = i_{min} : i : i_{max} \\ K_I = j_{min} : j : j_{max} \\ K_D = k_{min} : k : k_{max} \end{cases} \\
&if \quad e(t) = e(t)_{min} \\
&\qquad \begin{cases} K_{Po} = K_{Paccept} \\ K_{Io} = K_{Iaccept} \\ K_{Do} = K_{Daccept} \end{cases} \\
&else \quad \begin{cases} K_P = K_{Po+i} \\ K_I = K_{Io+j} \\ K_D = K_{Do+k} \end{cases}
\end{aligned} \tag{41}
$$

For the first loop, the range of parameters should be predefined. Besides, a reasonable value of the smallest division also needs to be determined. These values are used in the calculation and simulation processes. The optimal value (raw value) can be obtained once the condition related to minimizing the error signal is satisfied.

Table 1. Simulation parameters.

Description	Symbol	Value	Unit
Sprung mass	m_s	510	kg
Unsprung mass	m_u	54	kg
Spring coefficient	S	45,000	N/m
Damper coefficient	D	3700	Ns/m
Tire coefficient	T	174,000	N/m

The second loop is similar to the first loop. However, the range of values for this loop is reduced based on the initialized raw values.

Simulation results

The performance of the proposed hybrid PID-SMC strategy is characterized in simulations conducted in MATLAB/Simulink® 2021 environment running on a PC with core i9-12900K and 32GB RAM. The simulation parameters are given in Table 1. These parameters are determined based on mechanical simulation carried out in CARSIM® software.

Simulations are conducted for three cases corresponding to the four types of roughness on the road. In each case, four situations are considered. In the first situation, the vehicle uses a passive suspension system. The second situation involves an active suspension system with application of PID controller while in the third situation, SMC is applied to the active suspension system. The PID-SMC hybrid integrated controller is shown in the last situation.

In the first case, cyclic pavement excitation with a sinusoidal function is used as illustrated in Figure 4. The displacement of the vehicle body is also shown in this figure. The amplitude of oscillations in the vehicle is the largest and reaches up to 131.85 mm in the case when the vehicle only uses a mechanical suspension system. This value can be reduced to 51.02 and 40.56 mm if the vehicle uses the active suspension system controlled by PID or SMC algorithms respectively. When SMC algorithm is combined with PID algorithm, this value can be further reduced to only 8.98 mm. In addition to considering the maximum value of oscillations, the average values should also be considered when assessing vehicle oscillations. The average value is calculated for the case when the vehicle oscillates continuously. Based on Root Mean Square (RMS) criteria, the average value of the displacement can reach 87.32, 36.15, 28.67, and 6.32 mm respectively for the four situations under investigation.

The change in acceleration of the sprung mass over time represents the smoothness of vehicle's motion as shown in Figure 5. If acceleration is unreasonably high, vehicle comfort may be affected. In the first phase of
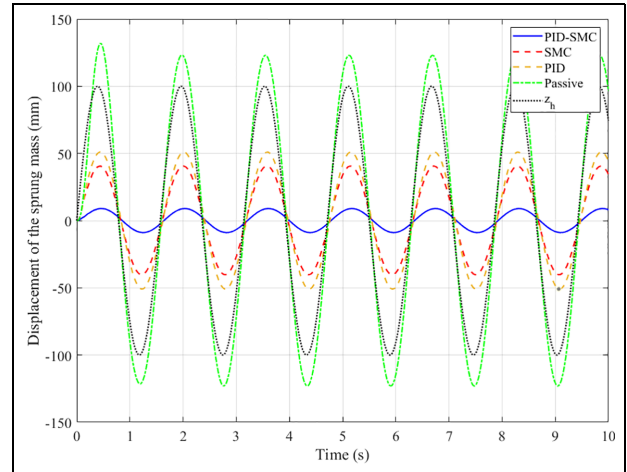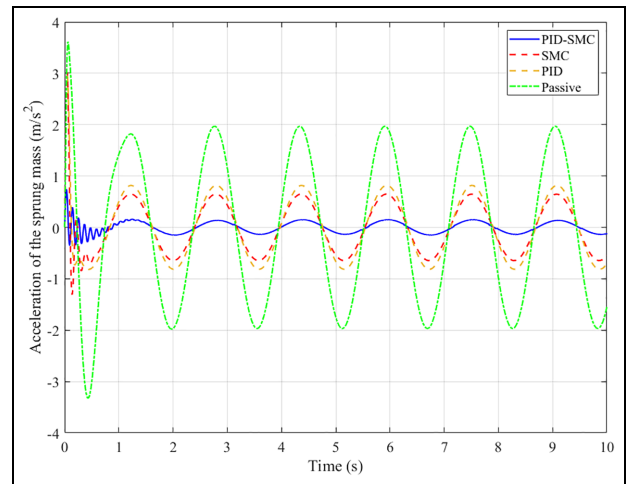

Figure 4. Sprung mass displacement – Case 1.

Figure 5. Sprung mass acceleration – Case 1.

the oscillation, the acceleration reaches its maximum value of $0.74 \, \text{m/s}^2$ (PID-SMC), $3.02 \, \text{m/s}^2$ (SMC), $2.96 \, \text{m/s}^2$ (PID), and $3.61 \, \text{m/s}^2$ (passive). The average value of acceleration is 0.11, 0.51, 0.62, and $1.48 \, \text{m/s}^2$ respectively for the four situations under consideration.

The vehicle is unstable when the wheel separates from the road surface. At that time, the vertical force at the wheel has reached zero. The greater the variation in the dynamic load, the higher the risk of the vehicle falling into instability. This problem can be resolved in a better way if the vehicle uses an active suspension system with the proposed hybrid PID-SMC algorithm. The change in dynamic load is not large as shown in Figure 6.

In the second case, a single trapezoidal form of pavement stimulus is used (see Figure 7) to determine the stability of the system after application of the excitation signal. The results indicate that displacement of the
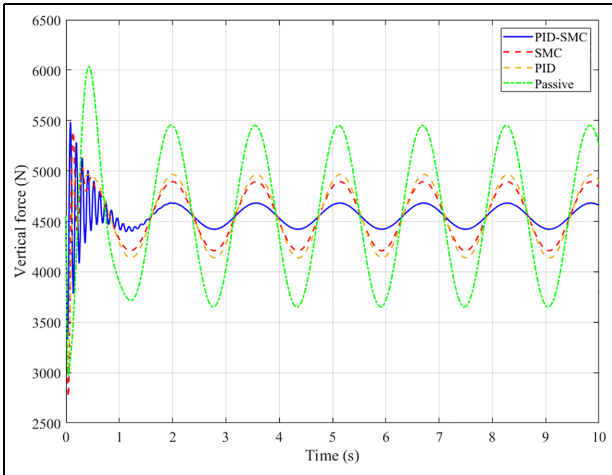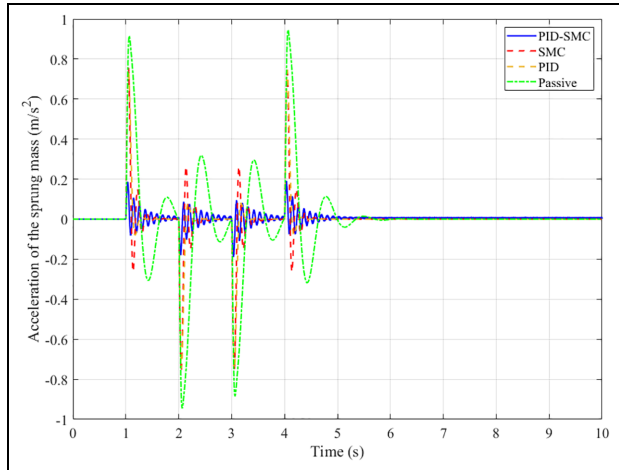
Figure 6. Vertical force – Case 1.

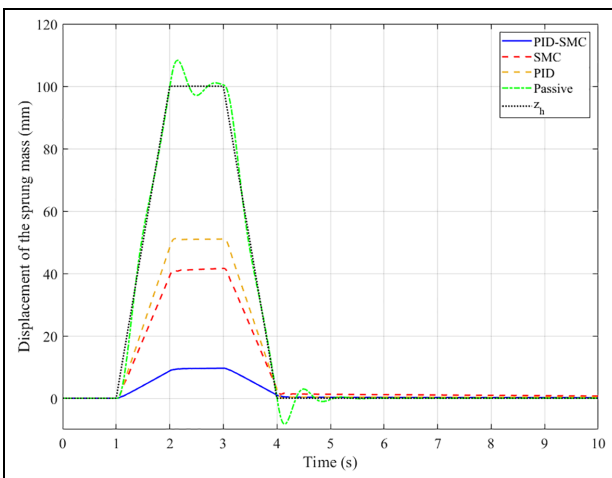**Figure 8.** Sprung mass acceleration – Case 2.

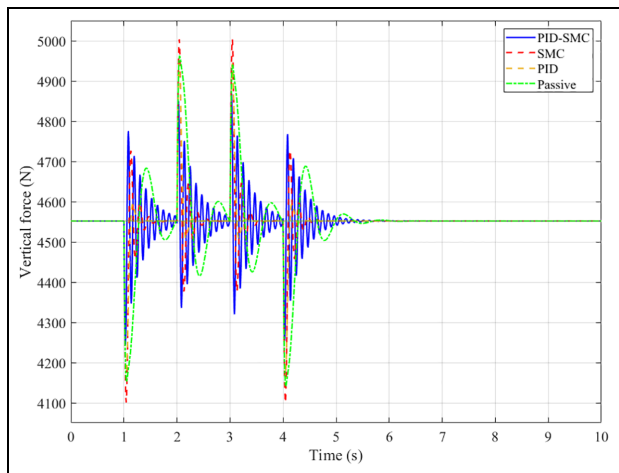**Figure 7.** Sprung mass displacement – Case 2.

Figure 9. Vertical force – Case 2.

vehicle body exhibits a huge peak when the vehicle does not have an active suspension system (Figure 7). These values gradually decrease corresponding to the other three situations. The maximum values of the four situations are found to be 9.63 mm (PID-SMC), 41.62 mm (SMC), 51.17 mm (PID), and 108.30 mm (passive), respectively. After the excitation signal from the road surface is ceased to zero, the vehicle body continues to oscillate with a small amplitude for a certain time if the vehicle only uses the passive suspension system. In contrast, the active suspension system offers more stable decay of oscillations. Since this is not a continuous excitation, therefore, the average value of the oscillations is not considered.

The changes in acceleration and vertical force are shown in Figures 8 and 9 respectively. The acceleration and the force tend to be opposite to each other. In this case, the sprung mass acceleration is not high for all the

situations because the acceleration and frequency of the excitation signal are quite small. This causes the value of the dynamic force at the wheel to change only within a small range. So, the vehicle is still in a steady state, and the interaction between the wheel and the road surface is always guaranteed.

In the above two cases, the amplitude and frequency of the stimulus are still not large. Therefore, the vehicle oscillation is not much affected. To investigate the oscillations more critically and comprehensively, the third case considers excitations with relatively larger frequencies and amplitudes as shown in Figure 10. The results indicate more variations in the vehicle oscillations.

The acceleration of the sprung mass can reach very large values of up to 9.90 m/s² corresponding to the fourth situation as shown in Figure 11. For the other situations, the maximum values of acceleration are found to be only 1.67, 6.73, and 6.60 m/s² respectively.
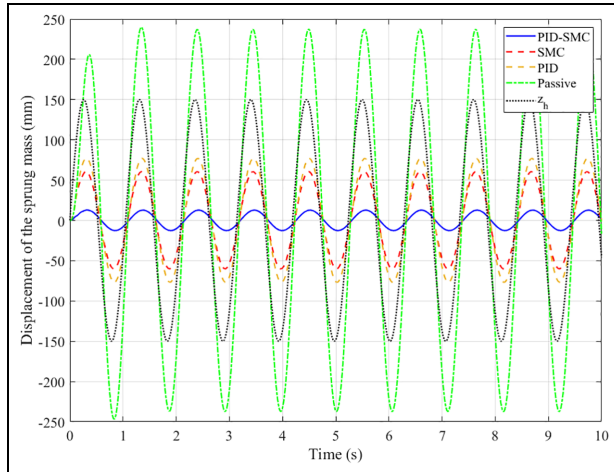
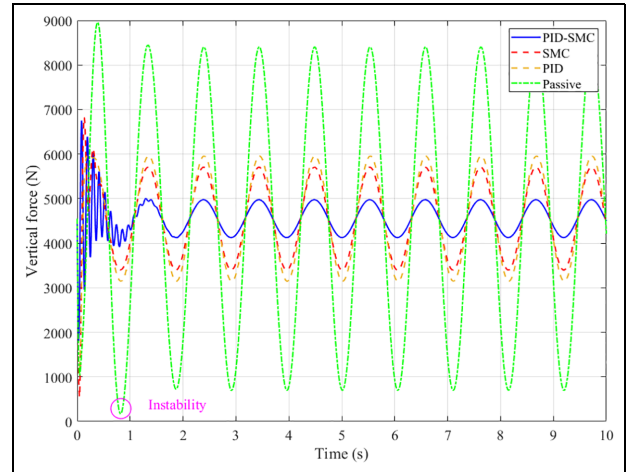**Figure 10.** Displacement of the sprung mass – Case 3.
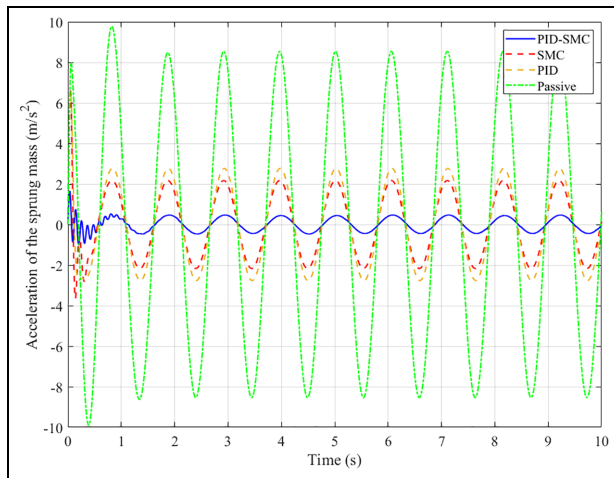

Figure 12. Vertical force – Case 3.

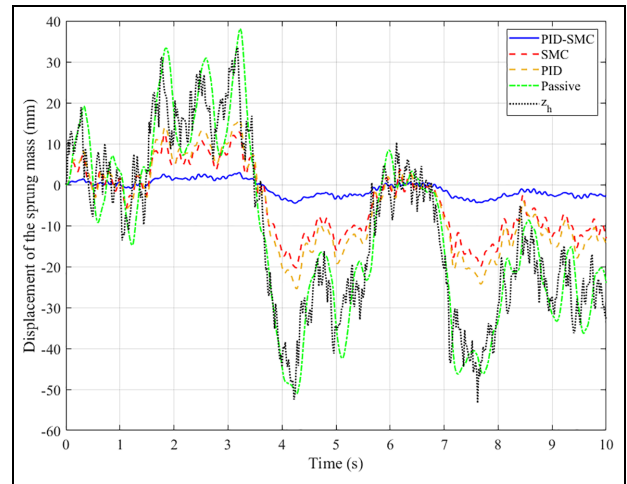**Figure 11.** Acceleration of the sprung mass – Case 3.

Figure 13. Displacement of the sprung mass – Case 4.

In this situation, the vertical force at the wheel can almost reach its limited value (approximately zero) if the vehicle uses only a conventional passive suspension system thus making the vehicle unstable. This is shown as an instability state in Figure 12. However, this state only lasts for a very small amount of time. If the amplitude and frequency of the stimulus continue to increase, the wheel may become completely detached from the road surface. In contrast to passive suspension, the stability of the vehicle is always ensured when the vehicle uses an active suspension system particularly when controlled by the proposed hybrid PID-SMC algorithm.

In the last case, a random pavement excitation is used. Referring to Figure 13, the signal has a frequency and an amplitude that change continuously over time. Therefore, it causes the vehicle body to oscillate continuously. The results in Figure 13 show that the maximum displacement of the car body can go up to 51.07 mm if the car only has a conventional suspension system. This value is reduced by about half, to 25.47 mm, when we use the active suspension system controlled by the traditional PID controller. This figure drops slightly to 20.34 mm if SMC controller takes the place of the PID controller. Finally, vehicle vibrations can be suppressed almost entirely once the suspension system is controlled by the hybrid algorithm proposed in this article (4.52 mm). Compared to the passive situation, the average displacement value of the PID-SMC situation is only about 8.94%.

In this case, the value of the vehicle body acceleration changes drastically. SMC algorithm causes the acceleration of the vehicle body to increase compared to the passive situation, while the value obtained from PID situation is approximately same as the passive situation. In contrast to this, the peak and average values of acceleration can be significantly reduced with the application of the proposed PID-SMC hybrid algorithm as evident from Figure 14. To achieve this, the
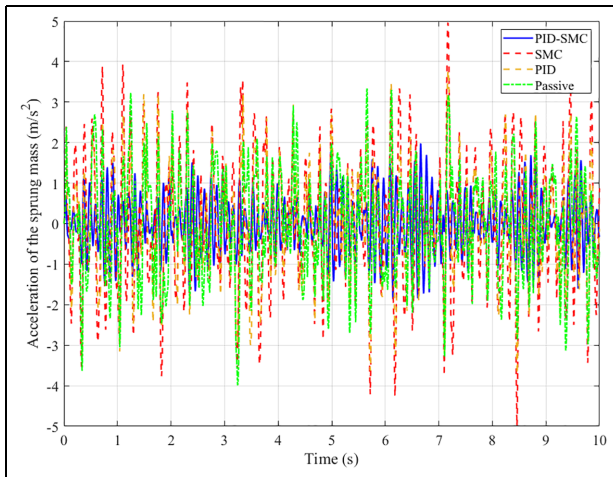
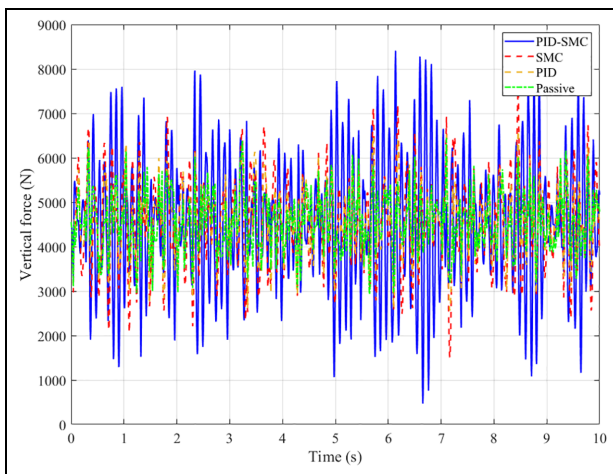**Figure 14.** Acceleration of the sprung mass – Case 4.

Figure 15. Vertical force – Case 4.

hydraulic actuator of the active suspension system needs to work harder, leading to a drastic change in the vertical force. This is a slight limitation of the algorithm proposed in this work. However, the system's stability is still guaranteed (Figure 15).

Overall, the results for the SMC or PID situations are similar with negligible errors. The efficiency of the suspension system can be significantly improved when we use the proposed hybrid controller as demonstrated in the present work.

The simulation results can be tabulated in a compact form. Tables 2 to 5 respectively present the results corresponding to Case 1–4. In fact, computing and processing systems onboard the vehicle often have more limited processing capabilities than high-performance personal computers with customized configuration. The limited onboard processing power can lead to delays in control. To solve this problem, we can combine some adaptive delay compensation techniques with the existing algorithm.

Conclusion

This research improves rider's comfort by reducing vehicle oscillations using an active suspension system. In particular, control of the suspension system is realized by proposing a proposed hybrid PID-SMC algorithm, which is developed based on quarter-model dynamics. Simulations results using three stimuli from road, each characterizing four situations, demonstrate that the active suspension system is capable of significantly reducing oscillations to provide better ride comfort. The maximum and average displacements of vehicle body as well as acceleration values have

Table 2. Case 1: Sine wave excitation with a small amplitude and frequency.

Parameter	Value	PID-SMC	SMC	PID	Passive
Displacement of the sprung mass (mm)	Maximum	8.98	40.56	51.02	131.85
	Average	6.32	28.67	36.15	87.32
Acceleration of the sprung mass (m/s^2)	Maximum	0.74	3.02	2.96	3.61
	Average	0.11	0.51	0.62	1.48
Vertical force of the wheel (N)	Minimum	3324.2	2757.5	2995.7	2969.0
	Average	4556.0	4565.1	4568.3	4615.7

Table 3. Case 2: Trapezoidal pulse excitation.

Parameter	Value	PID-SMC	SMC	PID	Passive
Displacement of the sprung mass (mm)	Maximum	9.63	41.62	51.17	108.30
	Average				
Acceleration of the sprung mass (m/s^2)	Maximum	0.19	0.76	0.75	0.95
	Average				
Vertical force of the wheel (N)	Minimum	4244.1	4100.5	4106.6	4140.9
	Average				

Table 4. Case 3: Sine wave excitation with a high amplitude and frequency.

Parameter	Value	PID-SMC	SMC	PID	Passive
Displacement of the sprung mass (mm)	Maximum	12.95	60.82	76.91	246.73
	Average	8.95	42.52	54.20	166.17
Acceleration of the sprung mass (m/s^2)	Maximum	1.67	6.73	6.60	9.90
	Average	0.35	1.61	2.01	6.11
Vertical force of the wheel (N)	Minimum	1799.7	547.2	1083.7	169.4
	Average	4575.6	4652.6	4688.1	5374.6

Table 5. Case 4: Random excitation.

Parameter	Value	PID-SMC	SMC	PID	Passive
Displacement of the sprung mass (mm)	Maximum	4.52	20.34	25.47	51.07
	Average	2.19	9.61	11.83	24.49
Acceleration of the sprung mass (m/s^2)	Maximum	1.98	4.99	3.77	3.99
	Average	0.68	1.56	1.28	1.26
Vertical force of the wheel (N)	Minimum	469.8	1505.4	2560.5	2933.6
	Average	4766.7	4657.4	4607.7	4595.5

decreased significantly by the application of the hybrid control algorithm. Moreover, the change in vertical force is also reduced using the proposed algorithm. Thus, the proposed hybrid algorithm overperforms than the passive system as well as an active suspension system controlled only with a PID or SMC algorithm. In near future, we plan to combine the fuzzy algorithm with the hybrid PID-SMC algorithm to further reduce chattering which occurs during some oscillation time.

ORCID iD

Tuan Anh Nguyen (iD) https://orcid.org/0000-0002-6064-2262

Data availability statement

The data generated or analyzed during this research are included in this published article.

References

1. Mehmood Y, Aslam J, Ullah N, et al. Robust fuzzy sliding mode controller for a skid-steered vehicle subjected to friction variations. *PLoS One* 2021; 16: e0258909.
2. Ahmad E, Iqbal J, Arshad M, et al. Predictive control using active aerodynamic surfaces to improve ride quality of a vehicle. *Electronics* 2020; 9: 1463.
3. Nguyen TA. Advance the stability of the vehicle by using the pneumatic suspension system integrated with the hydraulic actuator. *Lat Am J Solids Struct* 2021; 18: e403.
4. Ho CM, Tran DT, Nguyen CH, et al. Adaptive neural command filtered control for pneumatic active suspension with prescribed performance and input saturation. *IEEE Access* 2021; 9: 56855–56868.
5. Guowei D, Wenhao Y, Zhongxing L, et al. Sliding mode control of laterally interconnected air suspensions. *Appl Sci* 2020; 10: 4320.
6. Wei L, Lv H, Yang K, et al. A comprehensive study on the optimal design of magnetorheological dampers for improved damping capacity and dynamical adjustability. *Actuators* 2021; 10: 64.
7. Jin S, Deng L, Yang J, et al. A smart passive MR damper with a hybrid powering system for impact mitigation: an experimental study. *J Intell Mater Syst Struct* 2021; 32: 1452–1461.
8. Bai XL and Lei J. Active suspension control by output feedback through extended high-gain observers. *Ferroelectrics* 2019; 548: 185–200.
9. Meng Q, Chen CC, Wang P, et al. Study on vehicle active suspension system control method based on homogeneous domination approach. *Asian J Control* 2021; 23: 561–571.
10. Xia Y, Fu M, Li C, et al. Active disturbance rejection control for active suspension system of tracked vehicles with gun. *IEEE Trans Ind Electron* 2018; 65: 4051–4060.
11. Su X. Master–slave control for active suspension systems with hydraulic actuator dynamics. *IEEE Access* 2017; 5: 3612–3621.
12. Iqbal U, Samad A, Nissa Z, et al. Embedded control system for AUTAREP-a novel AUTonomous Articulated Robotic Educational Platform. *Tehnicki Vjesnik-Technical Gazette* 2014; 21: 1255–1261.

13. Mohammadikia R and Aliasghary M. Design of an interval type-2 fractional order fuzzy controller for a tractor active suspension system. *Comput Electron Agric* 2019; 167: 105049.

14. Moghadam-Fard H and Samadi F. Active Suspension System Control Using Adaptive Neuro Fuzzy (ANFIS) controller. *Int J Eng* 2015; 28: 396–401.

15. Ding X, Li R, Cheng Y, et al. Design of and research into a multiple-fuzzy PID suspension control system based on road recognition. *Processes* 2021; 9: 2190.

16. Bashir AO, Rui X, Abbas LK, et al. Ride comfort enhancement of semi-active vehicle suspension based on SMC with PID sliding surface parameters tuning using PSO. *J Control Eng Appl Inform* 2019; 21: 51–62.

17. Chiou JS, Tsai SH and Liu MT. A PSO-based adaptive fuzzy PID-controllers. *Simul Model Pract Theory* 2012; 26: 49–59.

18. Tan D, Lu C and Zhang X. Dual-loop PID control with PSO algorithm for the active suspension of the electric vehicle driven by in-wheel motor. *J Vibroengineering* 2016; 18: 3915–3929.

19. Aldair AA, Alsaedee EB and Abdalla TY. Design of ABCF control scheme for full vehicle nonlinear active suspension system with passenger seat. *Iran J Sci Technol Trans Electr Eng* 2019; 43: 289–302.

20. Nguyen TA. Improving the comfort of the vehicle based on using the active suspension system controlled by the double-integrated controller. *Shock Vib* 2021; 2021: 1–11.

21. Park M and Yim S. Design of static output feedback and structured controllers for active suspension with quarter-car model. *Energies* 2021; 14: 8231.

22. Wu JL. A simultaneous mixed LQR/H∞ control approach to the design of reliable active suspension controllers. *Asian J Control* 2017; 19: 415–427.

23. Nguyen ML, Tran TT, Nguyen TA, et al. Application of MIMO control algorithm for active suspension system: a new model with 5 state variables. *Lat Am J Solids Struct* 2022; 19: e435.

24. Haddar M. Intelligent optimal controller design applied to quarter car model based on non-asymptotic observer for improved vehicle dynamics. *Proc IMechE, Part I: J Systems and Control Engineering* 2021; 235: 929–942.

25. Ahmed M, Huq M and Ibrahim B. Investigating the effect of mass variation for sliding mode control of functional electrical stimulation aided sit-to-stand in paraplegia. In: *Proceedings of the 2019 IEEE 15th International Colloquium on Signal Processing & Its Applications (CSPA)*, Penang, Malaysia, 8–9 March 2019, pp.223–228. New York: IEEE.

26. Anjum M, Khan Q, Ullah S, et al. Maximum power extraction from a standalone photo voltaic system via neuro-adaptive arbitrary order sliding mode control strategy with high gain differentiation. *Appl Sci* 2022; 12: 2773.

27. Khan O, Pervaiz M, Ahmad E, et al. On the derivation of novel model and sophisticated control of flexible joint manipulator. *Revue Roumaine des Sciences Techniques-Serie Electrotechnique et Energetique* 2017; 62: 103–108.

28. Nguyen DN, Nguyen TA and Dang ND. A novel sliding mode control algorithm for an active suspension system considering with the hydraulic actuator. *Lat Am J Solids Struct* 2022; 19: e424.

29. Nguyen TA. Advance the efficiency of an active suspension system by the sliding mode control algorithm with five state variables. *IEEE Access* 2021; 9: 164368–164378.

30. Liu S, Zheng T, Zhao D, et al. Strongly perturbed sliding mode adaptive control of vehicle active suspension system considering actuator nonlinearity. *Veh Syst Dyn* 2022; 60: 597–616.

31. Iqbal J, Ullah MI, Khan AA, et al. Towards sophisticated control of robotic manipulators: experimental study on a pseudo-industrial arm. *Strojniški vestnik – Journal of Mechanical Engineering* 2015; 61: 465–470.

32. Golouje YN and Abtahi SM. Chaotic dynamics of the vertical model in vehicles and chaos control of active suspension system via the fuzzy fast terminal sliding mode control. *J Mech Sci Technol* 2021; 35: 31–43.

33. Ahmad S, Uppal AA, Azam MR, et al. Chattering free sliding mode control and state dependent Kalman filter design for underground gasification energy conversion process. *Electronics* 2023; 12: 876.

34. Pang H, Yang J and Liang J. On enhanced fuzzy sliding-mode controller and its chattering suppression for vehicle semi-active suspension system. SAE technical paper 2018-01-1403, 2018.

35. Rath JJ, Defoort M, Sentouh C, et al. Output-constrained robust sliding mode based nonlinear active suspension control. *IEEE Trans Ind Electron* 2020; 67: 10652–10662.

36. Singh D. Modeling and control of passenger body vibrations in active quarter car system: a hybrid ANFIS PID approach. *Int J Dyn Control* 2018; 6: 1649–1662.

37. Konoiko A, Kadhem A, Saiful I, et al. Deep learning framework for controlling an active suspension system. *J Vib Control* 2019; 25: 2316–2329.

38. Čorić M, Deur J, Xu L, et al. Optimisation of active suspension control inputs for improved vehicle ride performance. *Veh Syst Dyn* 2016; 54: 1004–1030.

39. Al Aela AM, Kenne JP and Mintsa HA. Adaptive neural network and nonlinear electrohydraulic active suspension control system. *J Vib Control* 2022; 28: 243–259.

40. Nguyen DN and Nguyen TA. Evaluate the stability of the vehicle when using the active suspension system with a hydraulic actuator controlled by the OSMC algorithm. *Sci Rep* 2022; 12: 19364.

41. Nguyen DN, Nguyen TA, Dang ND, et al. LQR control with the new triple in-loops algorithm for optimization of the tuning parameters. *Math Model Eng Probl* 2022; 9: 628–636.

42. Tran TTH, Nguyen TA, Hoang TB, et al. Optimizing the parameter of the LQR controller for active suspension system. In: Le AT, Pham VS, Le MQ, et al. (eds) *The AUN/SEED-net joint regional conference in transportation, energy, and mechanical manufacturing engineering. RCTEMME 2021*. Lecture Notes in Mechanical Engineering. Singapore: Springer, 2022, pp.260–270.

43. Nguyen TA. Design a new control algorithm AFSP (Adaptive Fuzzy – Sliding Mode – Proportional – Integral) for automotive suspension system. *Adv Mech Eng* 2023; 15: 13.